Controlled generation of intrinsic near-infrared color centers in 4H-SiC via proton irradiation and annealing

M. Rühl,[1,a)] C. Ott,[1] S. Götzinger,[2,3] M. Krieger,[1] and H. B. Weber[1]
[1]*Department Physik, Lehrstuhl für Angewandte Physik, FAU Erlangen-Nürnberg, D-91058 Erlangen, Germany*
[2]*Department Physik, Institut für Optik, Information und Photonik, FAU Erlangen-Nürnberg, D-91058 Erlangen, Germany*
[3]*Max Planck Institute for the Science of Light, D-91058 Erlangen, Germany*

(Received 25 June 2018; accepted 28 August 2018; published online 18 September 2018)

We report on the generation and annihilation of color centers in 4H silicon carbide (SiC) by proton irradiation and subsequent annealing. Using low-temperature photoluminescence (PL), we study the transformation of PL spectra for different proton doses and annealing temperatures. Among well reported defect signatures, we observe omnipresent but not yet identified PL signatures consisting of three sharp and temperature stable lines (denoted $TS_{1,2,3}$) at 768.8 nm, 812.0 nm, and 813.3 nm. These lines show a strong correlation throughout all measurement parameters, suggesting that they belong to the same microscopic defect. Further, a clear dependence of the $TS_{1,2,3}$ line intensities on the initial implantation dose is observed after annealing, indicating that the underlying defect is related to implantation induced intrinsic defects. The overall data suggest a sequential defect transformation: proton irradiation initially generates isolated silicon vacancies which are transformed into antisite vacancy complexes which are, in turn, transformed into presumably intrinsic-related defects, showing up as $TS_{1,2,3}$ PL lines. We present recipes for the controlled generation of these color centers. *Published by AIP Publishing.* https://doi.org/10.1063/1.5045859

As a wide bandgap semiconductor, silicon carbide (SiC) can serve as a host material for optically excitable point defects, termed color centers, emitting characteristic spectral signatures in the visible and near-infrared regime.[1] In recent years, the interest in such points like quantum systems grew dramatically due to their application as atomic-scale sensors[2,3] and single photon sources, both even at room temperature.[4,5] Compared to diamond, which is another frequently used material to host color centers,[6–8] SiC possesses significant advantages in terms of process technology and wafer-size availability making it an attractive candidate for future on-chip quantum technology.[9,10]

In this paper, we provide an extensive photoluminescence (PL) study of presumably intrinsic-related color centers embedded in a bulk SiC matrix. The formation of these defects is triggered by proton irradiation in a wide range of doses. Further, their formation and annihilation are investigated after thermal treatment. In order to ensure optical sensitivity to bulk color centers, we provide a strategy to efficiently suppress undesired optically active surface emitters.

We use high-purity semi-insulating 4H silicon carbide (HPSI 4H-SiC) from CREE, Inc. Under the investigated excitation wavelength of 532 nm, the unprocessed samples show numerous blinking spots at the sample surface [Fig. 1(a)] which will be denoted as near-surface emitters (NSEs) in the following. An obvious strategy to eliminate NSEs would be surface passivation. Surprisingly, passivation by thermal oxidation in the oxygen atmosphere around 800 °C leads to a significant increase in the NSE density [Fig. 1(c)], as previously reported.[16] When removing the oxide layer by a treatment with hydrofluoric acid, NSEs still dominate the luminescence. Due to the influence of the oxidation process, we assign the NSEs to oxygen related defects at the sample surface with a PL distributed between 600 nm and 700 nm (see also Ref. 17). While these objects are interesting themselves, their broad spectral distribution hampers the sensitivity to the underlying bulk color centers. In order to get rid of these NSEs, we opted for a controlled epitaxial graphene growth

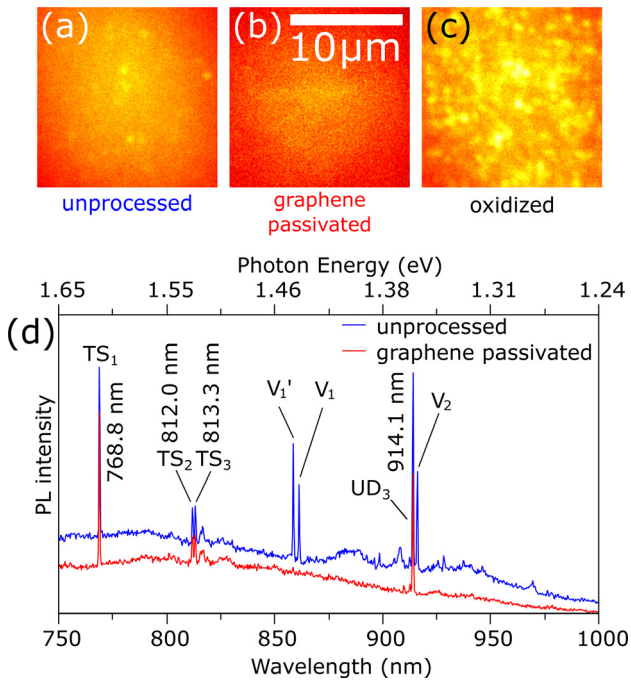

FIG. 1. (a)–(c) Images of the sample surface after different treatments: unprocessed, graphene passivated, and oxidized. (d) Low-temperature PL spectra before and after the graphene passivation step. Note that the V lines vanish after graphene growth.

a)Electronic mail: maxi.ruehl@fau.de

on the surface using argon-assisted thermal decomposition of SiC[18] (here: $T_{growth} = 1675\,^{\circ}C$). This has several consequences: (i) an atomically flat graphene layer grows which completely removes oxygen from the surface and protects the resulting ultra-flat surface from further oxidation. The result can be seen in Fig. 1(b) which reveals almost no NSEs. (ii) The graphene layer has virtually no photoluminescence and its transparency is spectrally flat at 97.7%.[19] Therefore, epitaxial graphene provides a well controlled window for optical studies of the underlying bulk color centers. (iii) The high temperature step that forms graphene removes the PL signature of silicon vacancies (V_{Si}) already present in the as-grown material. This effect is best reported in the spectra of unprocessed and graphene passivated samples displayed in Fig. 1(d) (elimination of the V_1', V_1, and V_2 line). Note that several other lines (in particular, $TS_{1,2,3}$ and UD_3, where TS stands for temperature stable) resist the high temperature anneal; these TS lines, yet unreported, will be a central topic of this study.

For the investigation of defect creation and annihilation, a proton irradiation (350 keV) is performed with various implantation doses on four quadrants side-by-side on the very same chip (not implanted, $10^{13}\,cm^{-2}$, $10^{14}\,cm^{-2}$, and $10^{15}\,cm^{-2}$). Afterwards, ensemble PL measurements are carried out for each implantation dose. Then, the sample is sequentially annealed at temperatures from 400 °C up to 1600 °C for 30 min and the PL measurement is repeated after each annealing step. The annealing up to 1000 °C is performed under vacuum; for higher temperatures, a different furnace with the argon atmosphere is used.

For the PL measurement, the sample is placed inside a liquid helium cryostat and cooled down to about 4 K. A continuous wave 532 nm (frequency doubled Nd:YVO_4) laser polarized perpendicular to the crystal c-axis is used for sample excitation. The laser beam is focused onto the back focal plane of the microscope objective using a widefield lens resulting in a collimated beam at the sample surface for ensemble excitation. Emitted PL is then collected by a microscope objective with NA = 0.75 and recorded either by an Andor Shamrock 500i spectrograph connected to an Andor Newton 920 open-electrode CCD camera or by a Hamamatsu ORCA Flash 4 V2 sCMOS imaging camera.

Figure 2 shows the PL spectra directly after proton irradiation. The most prominent features in the spectra are the V lines whose intensities strongly increase with increasing implantation dose. The V lines are accompanied by broad phonon sidebands. These signatures have been discussed by Janzén *et al.* (Ref. 11) and have been assigned to the isolated silicon vacancy (V_{Si}).[10] This point defect has been intensively studied as a single photon source.[20–23] Due to the inequivalent lattice sites in 4H-SiC, the V_{Si} appears as several lines (V_1', V_1, and V_2, see Fig. 2 and Table I). In previous studies, V_{Si} defects have predominantly been created by electron and neutron irradiation requiring large scale facilities.[1,22] Here, using the much more common technique of ion implantation in order to irradiate the samples with protons, we can generate V_{Si} in controlled amounts within the implantation depth of about 2.5 μm. When a moderate anneal between 400 °C and 600 °C is carried out, the V lines are the dominant spectral features that scale with proton irradiation

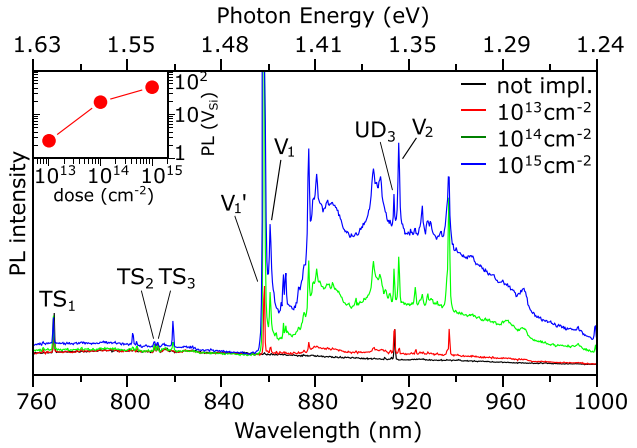

FIG. 2. PL spectra after proton irradiation with increasing implantation doses before annealing. The inset shows the PL intensity of the V_{Si} signature vs. implanted proton dose normalized to the V_{Si} PL corresponding to the lowest proton dose. Note that, in contrast to the V lines, the $TS_{1,2,3}$ lines are not affected by the irradiation before annealing.

dose (see inset in Fig. 2). In this temperature range, the TS lines are not yet affected by the anneal. They occur as a set of three lines $TS_{1,2,3}$ with wavelengths listed in Table I. Further, we observe a set of peaks with rather weak luminescence that increases in PL intensity with increasing proton irradiation dose, termed AB lines (see Table I). These AB lines have been assigned to the intrinsic carbon antisite vacancy pair (C_{Si}-V_C).[5,12] At the longest investigated wavelengths, another PL signature is observable, one of the four UD_2 lines.[13] This signature originates from the divacancy V_{Si}-V_C[4] (see again Table I) and is strongly suppressed by the low quantum efficiency (<5%) of the spectrometer at 1078.3 nm.

Starting from this initial situation, we now focus on the transformation of intrinsic defects during high temperature annealing. It is already reported that the V_{Si} transforms into the C_{Si}-V_C defect at elevated temperatures by moving a substitutional carbon atom into the V_{Si}[5,24] which manifests as an increase in the AB lines. Indeed, in our experiments, we observe a strong decrease in the V_{Si} PL accompanied by a simultaneous increase in AB intensity after annealing at temperatures above 600 °C. Concurrently, the UD_2 PL increases

TABLE I. Overview of experimentally observed PL signatures in this study.

Signature	Origin	PL line	λ (nm)	E_λ (meV)
V lines	V_{Si} (Refs. 10 and 11)	V_1'	858.7	1443.9
		V_1	861.3	1439.5
		V_2	916.1	1353.4
AB lines	C_{Si}-V_C (Refs. 5 and 12)	A_1	648.5	1911.9
		B_2	672.8	1842.8
		B_3	675.0	1836.8
		B_4	676.3	1833.3
UD_2 lines	V_{Si}-V_C (Refs. 4 and 13)	UD_2	1078.3	1149.8
UD_3 lines	Unknown (Refs. 14 and 15)	UD_3	914.1	1356.4
TS lines	Unknown	TS_1	768.8	1612.7
		(TS_1')	769.2	1611.9
		(TS_1'')	768.7	1612.9
		TS_2	812.0	1526.9
		TS_3	813.3	1524.5
		(TS_3')	813.5	1524.1

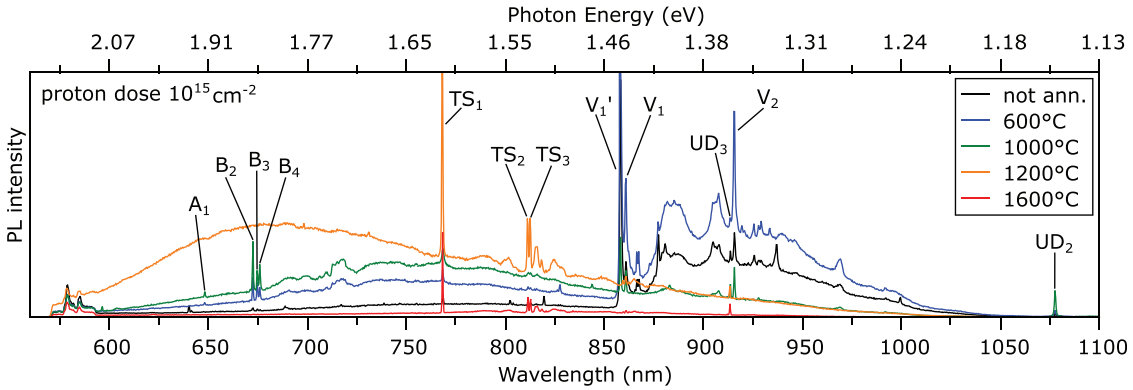

FIG. 3. Evolution of PL spectra after proton irradiation for various annealing temperatures. The dominant PL lines occurring through the annealing steps are labelled and listed in Table I. Note that after 1600 °C anneal, the TS lines and the UD_3 line remain the only considerable PL features in the spectrum.

in this annealing temperature region as well, suggesting the formation of V_{Si}-V_C at the expense of V_{Si}. For the AB lines and the UD_2 line, the transformation is completed after annealing at 1000 °C. This becomes visible in raw spectra (Fig. 3) as well as in the evolution of PL line intensities shown in Fig. 4(b).

When going to even higher annealing temperatures, another modification process takes place: While the AB lines in the PL spectra vanish above 1200 °C, as a sudden the yet unaffected TS lines increase drastically in intensity [see again Figs. 3 and 4(b)]. This evolution as a function of annealing temperature suggests the following transformation of PL signatures:

$$\text{V lines}_{(V_{Si})} \rightarrow \text{AB lines}_{(C_{Si}\text{-}V_C)} \rightarrow \text{TS lines}_{(\text{unkn.})}.$$

This PL transformation, in turn, suggests the reaction of the corresponding defects. Comparing AB and UD_2 line evolution [Fig. 4(b)], the UD_2 line is already strongly reduced when the TS intensity is still unaffected. Hence, a transformation from AB lines to TS lines is the more reasonable transformation process. The drastical increase in the background signal around 600 nm–800 nm (Fig. 3) is dependent on the irradiation dose and might be related to the TS formation. Above 1200 °C annealing temperature, no further transformation of PL lines is observed although the TS line intensities slightly decrease. In particular, this final result explains the initial occurrence of TS lines after graphene growth at 1675 °C. Note that based on PL results only, the microscopic defect transformation remains speculative, and further investigations like EPR and theory are required. In particular, already existing hidden extrinsic defects could also play a role in the formation of these defects. Nevertheless, the clear proton dose dependence observed underscores the intrinsic-related nature of the TS signature. With the aim of giving further hints for complementary studies, we now focus on a detailed analysis of the TS lines.

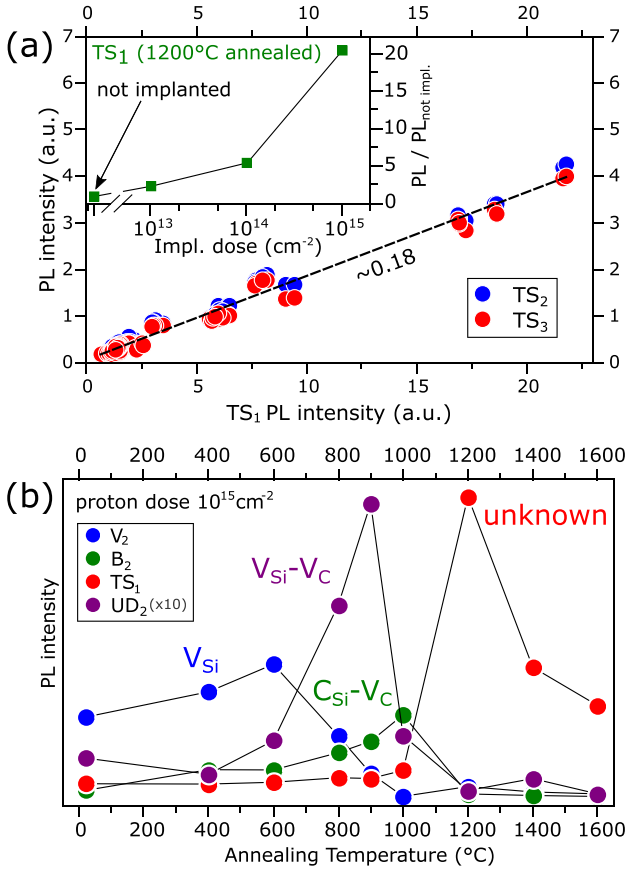

FIG. 4. (a) PL line intensities of signatures $TS_{2,3}$ vs. TS_1 for all investigated annealing temperatures and implantation doses. Note that the $TS_{2,3}$ line intensities scale with the TS_1 intensity (proportional to 0.18). The inset shows the TS_1 line intensity after 1200 °C annealing for different proton irradiation doses normalized to the intensity without irradiation. (b) Line intensities of the main PL signatures versus annealing temperatures. Note that the UD_2 intensity is scaled by a factor of 10.

Figure 4(a) shows the relationship between the PL intensities of the $TS_{2,3}$ line and TS_1 line. For all investigated measurement parameters (in particular, annealing temperatures and implantation doses), the PL intensities of TS_2 and TS_3 keep a fixed intensity ratio of about 0.18 compared to TS_1. This is clearly shown in the linear dependence between TS_1 and TS_2/TS_3 in Fig. 4(a). We therefore conclude that the multiplet $TS_{1,2,3}$ belongs to the same defect. Further, the inset in Fig. 4(a) shows the dependence of the TS signature PL intensity (after annealing) on the initially performed proton irradiation dose, suggesting that intrinsic defects are involved in the TS formation.

A high resolution analysis of the spectral composition of the $TS_{1,2,3}$ lines reveals that the TS_1 and the TS_3 lines show a fine structure that is displayed in Fig. 5 and listed in Table I. Due to the spectral proximity, we tentatively assign the satellites TS_1' and TS_1'' as well as TS_3' to the TS_1 and TS_3 line, respectively. We emphasize that further data are required to

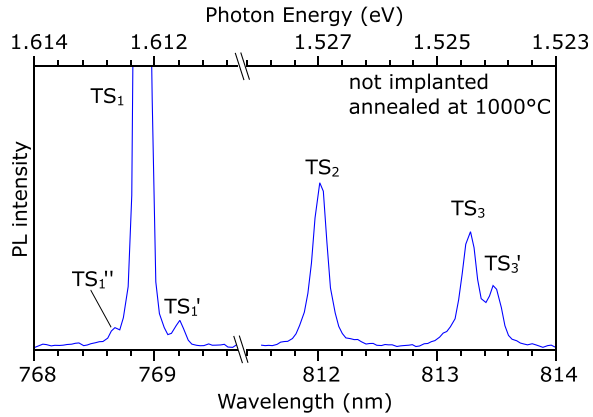

FIG. 5. High resolution spectra of the $TS_{1,2,3}$ signature. TS_1 and TS_3 show a fine structure: TS_1 shows two possibly related satellites, TS_1' and TS_1''. The TS_3 line shows a pronounced secondary line shifted towards larger wavelengths. The line width (FWHM) of TS_1 (≈85 pm) is limited by the resolution of our spectrometer, whereas the TS_2 line width (≈165 pm) is slightly above the resolution limit.

confirm this assignment. TS_1' and TS_1'' contribute only a few percent to the total TS_1 line intensity, as opposed to the TS_3' line, which accounts for about 1/3 of the total line intensity. Remarkably, the $TS_{1,2,3}$ ZPLs are accompanied by a very weak phonon side band resulting in a Debye-Waller factor (DWF) of about 45%. This indicates that the color center, as a quantum system, couples weakly to the dissipative environment. Compared to the DWF of V_{Si}, about 25%, this is very favorable. When further comparing the PL line sequence, a qualitative difference occurs: the V_{Si} has a double line structure (V_1', V_1) close to 860 nm and a single line (V_2) at larger wavelengths, whereas the TS_1 represents the single line followed by the double line $TS_{2,3}$ at larger wavelengths. When assigning these lines to point defects, the splitting between TS_1 and $TS_{2,3}$ presumably roots in inequivalent lattice sites (cubic/hexagonal) of the 4H-SiC crystal and the fine splitting between TS_2 and TS_3 may result from the local defect symmetry. The origin of the splitting and the spectral weight of these lines are currently unknown but may be a hint for their identification.

Summarizing, we performed low-temperature ensemble PL measurements at proton irradiated 4H-SiC and investigated the evolution of spectroscopic features for subsequent annealing temperatures. Besides the known V, AB, and $UD_{2,3}$ lines, dominant and yet unidentified spectral signatures occurred: A multiplet of three TS lines, capable of resisting the highest annealing temperature investigated. The TS lines keep a fixed intensity ratio over all irradiation doses and annealing temperatures, an observation which suggests that they are the PL signature of the same point defect on different lattice sites or with different local symmetries. Interestingly, our experiments starting with defect generation by proton irradiation plus sequential annealing steps reveal the genesis of the observed defects: After proton irradiation, first V_{Si} are generated which are converted into C_{Si}-V_C and V_{Si}-V_C at intermediate temperatures of about 1000 °C. Their spectroscopic signature vanishes at 1200 °C and is replaced by the presented TS lines. This suggests that the TS lines belong to an intrinsic or an intrinsic-related point defect presumably generated out of C_{Si}-V_C. Altogether, the manuscript presents recipes for controlled generation of intrinsic related color centers in 4H-SiC: A maximum intensity of V_{Si} related lines is obtained after annealing at 600 °C, UD_2 at 900 °C, AB lines at 1000 °C, and TS lines at 1200 °C. The line intensities are well controlled by the proton irradiation dose.

This work was supported by the Deutsche Forschungsgemeinschaft within the Project No. WE3542/10-1. We acknowledge useful discussions with Michel Bockstedte.

[1]T. C. Hain, F. Fuchs, V. A. Soltamov, P. G. Baranov, G. V. Astakhov, T. Hertel, and V. Dyakonov, J. Appl. Phys. **115**, 133508 (2014).
[2]F. Dolde, H. Fedder, M. W. Doherty, T. Nöbauer, F. Rempp, G. Balasubramanian, T. Wolf, F. Reinhard, L. C. L. Hollenberg, F. Jelezko, and J. Wrachtrup, Nat. Phys. **7**, 459 (2011).
[3]R. S. Schoenfeld and W. Harneit, Phys. Rev. Lett. **106**, 030802 (2011).
[4]W. F. Koehl, B. B. Buckley, F. J. Heremans, G. Calusine, and D. D. Awschalom, Nature **479**, 84 (2011).
[5]S. Castelletto, B. C. Johnson, V. Ivády, N. Stavrias, T. Umeda, A. Gali, and T. Ohshima, Nat. Mater. **13**, 151 (2014).
[6]T. Müller, C. Hepp, B. Pingault, E. Neu, S. Gsell, M. Schreck, H. Sternschulte, D. Steinmüller-Nethl, C. Becher, and M. Atatüre, Nat. Commun. **5**, 3328 (2014).
[7]T. Iwasaki, F. Ishibashi, Y. Miyamoto, Y. Doi, S. Kobayashi, T. Miyazaki, K. Tahara, K. D. Jahnke, L. J. Rogers, B. Naydenov, F. Jelezko, S. Yamasaki, S. Nagamachi, T. Inubushi, N. Mizuochi, and M. Hatano, Sci. Rep. **5**, 12882 (2015).
[8]J. D. Breeze, E. Salvadori, J. Sathian, N. M. Alford, and C. W. M. Kay, Nature **555**, 493 (2018).
[9]F. Fuchs, V. A. Soltamov, S. Väth, P. G. Baranov, E. N. Mokhov, G. V. Astakhov, and V. Dyakonov, Sci. Rep. **3**, 1637 (2013).
[10]V. Ivády, J. Davidsson, N. T. Son, T. Ohshima, I. A. Abrikosov, and A. Gali, Phys. Rev. B **96**, 161114 (2017).
[11]E. Janzén, A. Gali, P. Carlsson, A. Gällström, B. Magnusson, and N. Son, Mater. Sci. Forum **615–617**, 347 (2009).
[12]J. W. Steeds, Phys. Rev. B **80**, 245202 (2009).
[13]B. Magnusson and E. Janzén, Mater. Sci. Forum **483–485**, 341 (2005).
[14]M. Wagner, B. Magnusson, W. M. Chen, and E. Janzén, Phys. Rev. B **66**, 115204 (2002).
[15]D. Riedel, F. Fuchs, H. Kraus, S. Väth, A. Sperlich, V. Dyakonov, A. A. Soltamova, P. G. Baranov, V. A. Ilyin, and G. V. Astakhov, Phys. Rev. Lett. **109**, 226402 (2012).
[16]A. Lohrmann, S. Castelletto, J. R. Klein, T. Ohshima, M. Bosi, M. Negri, D. W. M. Lau, B. C. Gibson, S. Prawer, J. C. McCallum, and B. C. Johnson, Appl. Phys. Lett. **108**, 021107 (2016).
[17]A. Lohrmann, N. Iwamoto, Z. Bodrog, S. Castelletto, T. Ohshima, T. Karle, A. Gali, S. Prawer, J. McCallum, and B. Johnson, Nat. Commun. **6**, 7783 (2015).
[18]K. V. Emtsev, A. Bostwick, K. Horn, J. Jobst, G. L. Kellogg, L. Ley, J. L. McChesney, T. Ohta, S. A. Reshanov, J. Röhrl, E. Rotenberg, A. K. Schmid, D. Waldmann, H. B. Weber, and T. Seyller, Nat. Mater. **8**, 203 (2009).
[19]P. Goncalves and N. Peres, *An Introduction to Graphene Plasmonics* (World Scientific Publishing Company, 2016).
[20]H. Kraus, D. Simin, C. Kasper, Y. Suda, S. Kawabata, W. Kada, T. Honda, Y. Hijikata, T. Ohshima, V. Dyakonov, and G. V. Astakhov, Nano Lett. **17**, 2865 (2017).
[21]J. Wang, X. Zhang, Y. Zhou, K. Li, Z. Wang, P. Peddibhotla, F. Liu, S. Bauerdick, A. Rudzinski, Z. Liu, and W. Gao, ACS Photonics **4**, 1054 (2017).
[22]F. Fuchs, B. Stender, M. Trupke, D. Simin, J. Pflaum, V. Dyakonov, and G. V. Astakhov, Nat. Commun. **6**, 7578 (2015).
[23]M. Widmann, S.-Y. Lee, T. Rendler, N. T. Son, H. Fedder, S. Paik, L.-P. Yang, N. Zhao, S. Yang, I. Booker, A. Denisenko, M. Jamali, S. A. Momenzadeh, I. Gerhardt, T. Ohshima, A. Gali, E. Janzén, and J. Wrachtrup, Nat. Mater. **14**, 164 (2015).
[24]M. Bockstedte, A. Mattausch, and O. Pankratov, Phys. Rev. B **69**, 235202 (2004).